Proceedings of ASME Turbo Expo 2023
Turbomachinery Technical Conference and Exposition
GT2023
June 26-30, 2023, Boston, Massachusetts

GT2023-103128

NASA SMALL ENGINE COMPONENTS COMPRESSOR TEST FACILITY: HIGH EFFICIENCY CENTRIFUGAL COMPRESSOR VANELESS DIFFUSER AND TRANSITION DUCT CONFIGURATIONS

Herbert M. Harrison
NASA Glenn Research Center
Cleveland, OH
herbert.harrison@nasa.gov

Ezra O. McNichols
NASA Glenn Research Center
Cleveland, OH

Matthew R. Blaha
HX5 Sierra
Cleveland, OH

ABSTRACT

The original vaned configuration of the High Efficiency Centrifugal Compressor (HECC) was developed with aggressive design targets to facilitate advancement of state-of-the-art technology in gas turbine compressors. This work documents modifications to the Small Engine Components Compressor Test Facility to support testing of the HECC vaneless diffuser and transition duct configurations, both of which are open geometries. These configurations were developed as follow-up studies to improve understanding of the differences between the predicted and actual performance of the original HECC vaned diffuser stage. Specifically, the vaneless diffuser was designed to provide the impeller with ideal exit conditions such that the impeller performance could be isolated from downstream stationary components, and the additively manufactured transition duct inlet configuration enables investigation into the effects of the inlet flow path on the stage performance. Features of note in the facility are active clearance control, bleed flow regulation, modular inlet configurations, and steady-state and fast-response instrumentation throughout the flow path. Details of the facility and instrumentation are presented as well as the baseline performance of the compressor stage. The geometry, performance, and detailed aerodynamic data have been made available to the public at https://storage.googleapis.com/hecc-data/NASA-HECC-Data-Archive.zip.

Keywords: centrifugal compressor, impeller, vaneless diffuser, transition duct.

NOMENCLATURE

A	area
r	radius

SUBSCRIPTS

1	impeller leading edge
$mean$	mean value
x	axial coordinate

ACRONYMS

APU	auxiliary power unit
HECC	High Efficiency Centrifugal Compressor
HMI	human machine interface
BLM	baseline metal (inlet)
BLP	baseline plastic (inlet)
MH	modified hub (inlet)
PLC	programmable logic controller
TPR	total pressure ratio
TTR	total temperature rise ratio

1. INTRODUCTION

Despite decades of research, accurate and reliable prediction of centrifugal compressor performance and operability remains a challenge for the gas turbine community. Traditional design techniques based on meanline or two-dimensional methods rely heavily on empirical models and are closely guarded by the organizations that own them. Moreover, these traditional models are often unreliable when extended beyond the bounds of the experimental correlations on which they are based. Modern 3D numerical simulations are commonly developed with publicly available turbulence models and enable a much greater level of insight into the centrifugal compressor flow field. However, extensive research in the public domain has shown that performance prediction of centrifugal compressors with these

advanced techniques is unreliable, as well. In fact, existing experimental data as well as extreme care are necessary to accurately capture the centrifugal compressor flow field, and these prerequisites usually render true prediction and design with 3-D simulations unrealistic [1,2].

Centrifugal compressors present an amalgamation of many of the scenarios in which turbulence models for 3-D simulations develop inaccuracies: flow path curvature, rotating reference frames, adverse pressure gradients, and high levels of mixing are all present. Because numerical methods cannot be relied upon without experimental validation, as well as to improve the accuracy of those methods, open-access, experimental compressor data are invaluable in the effort to advance the forefront of compressor technology. The High Efficiency Centrifugal Compressor (HECC) program fills this niche of an open data set and, as given by Medic et al. [1], was developed with the following goals:

- identification of key technical barriers in the advancement of state-of-the-art of small centrifugal compressor stages,
- delineation of measurements required to provide insight into the flow physics associated with technical barriers,
- design, fabrication, installation, and testing of a state-of-the-art research compressor that is representative of the rear stage of an axial-centrifugal aero-engine,
- and acquisition of detailed aerodynamic performance and research quality data to clarify flow physics and establish detailed data sets for future application.

Since initiation of the test program in the late 2000s, the HECC test article has been used for multiple test campaigns in various configurations and has functioned as a valuable research vehicle for investigation into various topics of interest in the gas turbine community. The unique aspects of the HECC test article and the Small Engine Components Compressor Test Facility support investigations into impeller-diffuser interactions, surge and stall, tip clearance effects, and inlet distortion. Additionally, the facility supports the acquisition of velocity data with nonintrusive measurement techniques. Following is a review of the relevant topics.

Impeller-diffuser interactions are the many flow phenomena that develop due to the coupling of the rotating impeller and stationary diffuser. Generally, the efficiency of a centrifugal compressor stage is less than that of the isolated components due to impeller-diffuser interactions. As such, impeller-diffuser interactions occur in all centrifugal compressors which utilize diffusers, although the interactions are of much greater import in stages with vaned diffusers rather than vaneless diffusers. Impeller-diffuser interactions consist of two major aspects: the effect of the impeller on the diffuser and the effect of the diffuser on the impeller.

The effect of the impeller on the diffuser is characterized by viscous and potential effects and is generally considered to be the more important of the interactions [3]. The impeller ejects a jet-wake flow structure that varies temporally as well as spatially in the spanwise and pitchwise directions [4–7], and the unsteady, distorted nature of the impeller exit flow affects the ability of the diffuser to recover static pressure [2,8,9]. Additionally, the levels of unsteadiness output from the impeller are key to the mixing process in the diffuser passages [2,3]. The complex flow field passed from the impeller generates losses in the diffuser as a result of the impeller blade wakes, variation of velocity and inlet flow angle, and intense mixing in the vaneless space. Significant loss occurs in the mixing process between the impeller trailing edge and diffuser throat. Once downstream of the diffuser throat, the passage flow becomes both more uniform and steady [9–11].

The diffuser in turn creates an upstream potential disturbance in the impeller. Even vaneless diffusers affect the upstream impeller potential flow to a small extent, and vaned diffusers magnify this effect by adding unsteady pressure disturbances from the passage of impeller blades by the diffuser vanes. The interactions between the impeller and diffuser in a centrifugal compressor have been shown to be a strong function of radial gap where the intensity of interaction increases as the radial gap size decreases. The intensity of impeller-diffuser interactions is greater in modern machines due to smaller radial gaps and likewise greater potential effects [12,13]. While the effect of the impeller and diffuser on one another is a known phenomenon and has been extensively documented, predicting the magnitude of the interaction and effects thereof on the stage performance remain difficult [1].

Surge and stall limit the low-flow side of the compressor map, and an understanding of these instability phenomena is necessary for the development of centrifugal compressors with both adequate operating range and desired efficiency. In centrifugal compressors with vaned diffusers, low-flow instability usually manifests as surge with significant or global reversed flow, and until recently, the vaned diffuser was generally thought to be the stability-limiting component of the stage [14–18]. However, some researchers have begun to observe that surge signature of high-speed machines varies with operating speed [19,20], and more specifically, the impeller tip relative Mach number [21,22]. At high speeds, Lou et al. found the impeller leading edge shock nearly eliminated impeller inlet recirculation, and the presence or absence of inlet recirculation was critical to the stability of the stage. Additional research is needed to corroborate these recent findings concerning compressor stability as well as to understand the implications for various map-width enhancement techniques [23].

The effect of tip clearance in axial and centrifugal compressors continues to be an area of interest due to the decreasing size of aeroengines: as the size of the engine core decreases, the clearance values reach an asymptote, and the clearance gap becomes a larger percentage of the hub-to-shroud span. In centrifugal compressors, the compressor efficiency and pressure ratio decrease with increasing tip clearance [24]. The efficiency penalty as a function of tip clearance gap is usually linear, and the slope of the linear fit varies between designs as well as corrected speed [24–26]. Additional research is needed to facilitate a more thorough understanding of the impact of tip clearance on the impeller exit/diffuser inlet flow, as well as the effect on component performance.

Novel aircraft designs are being explored with the goal of improving propulsive efficiency. However, these innovative airframe architectures often result in performance penalties for the gas turbine generator due to the presence of inlet distortion which may inhibit with work input of rotors and pressure recovery of stators [27,28]. Additionally, sectors of the gas turbine in the distorted region operate at different corrected conditions than the undistorted regions, which degrades operability in addition to performance [29,30]. Inlet distortion present in hybrid electric engines and auxiliary power units (APUs) degrades the stable operating range of the compression components. This is especially a concern for centrifugal compressors which often have narrow ranges of stable operation between choke and instability with clean inlet flow. Developing comprehensive data sets to understand the impact of inlet distortion on compressor performance will facilitate the advancement of future airframes and power plants.

The research activities conducted with the HECC test article will utilize the numerous capabilities of the Small Engine Components Compressor Test Facility to investigate a wide array of phenomena in centrifugal compressors with the goal of improving design techniques and analysis tools for the aerospace community. Topics ranging from impeller-diffuser interactions to inlet distortion will be considered, and an ongoing upgrade to the facility will enable velocity data acquisition at the impeller exit. The present work describes and documents the HECC test article and CE-18 facility infrastructure at the NASA Glenn Research Center and serves as an update to the original facility report published in 1992 by Brokopp and Gronski [31].

2. FACILITY INFRASTRUCTURE

A diagram of the Small Engine Components Compressor Test Facility in the Engine Research Building at NASA Glenn Research center, colloquially referred to by its room number CE-

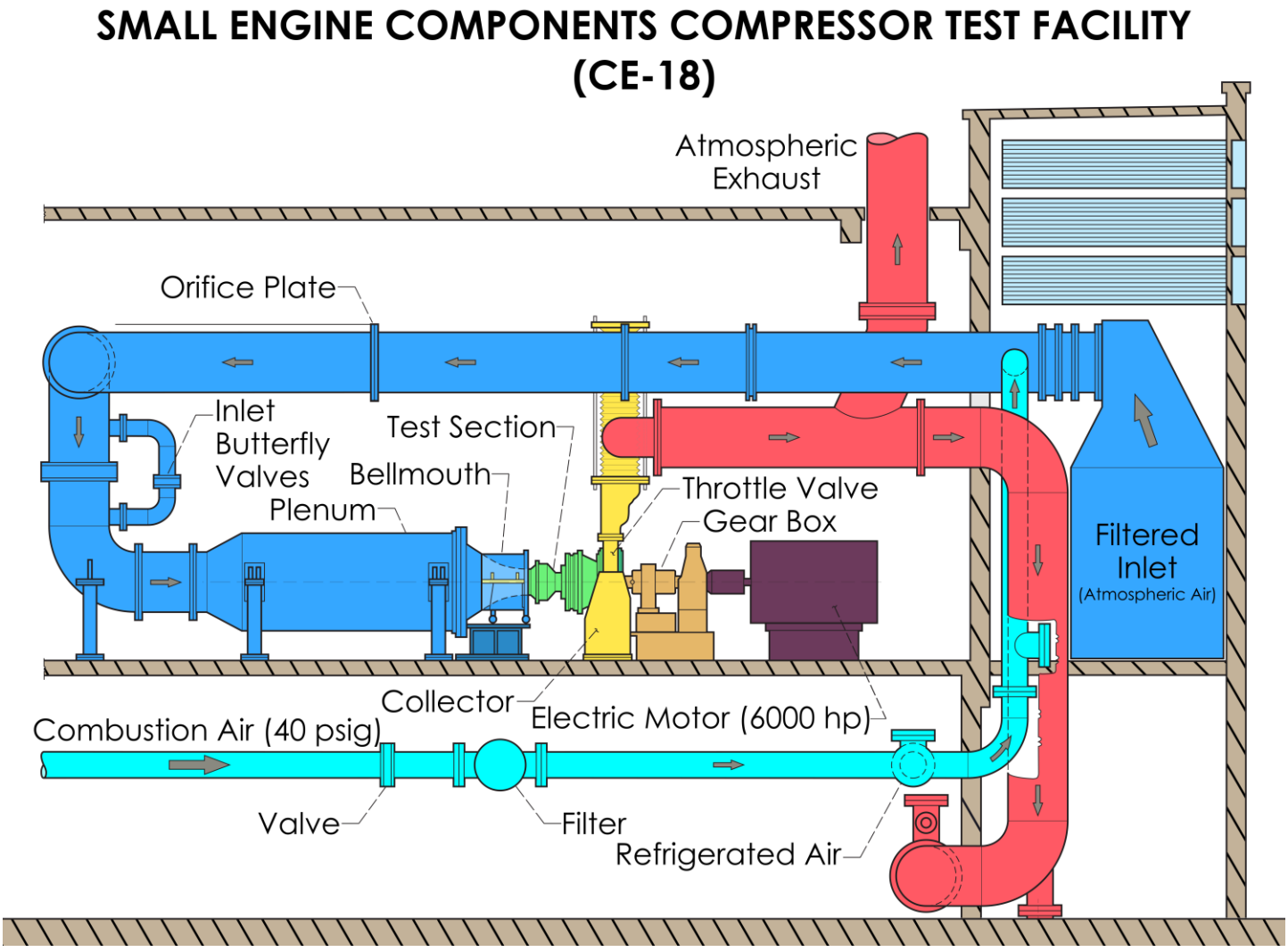

FIGURE 1. NASA SMALL ENGINE COMPONENTS COMPRESSOR TEST FACILITY; COMMONLY REFERRED TO AS CE-18.

18, is shown in Figure 1. The test article (green) is driven by a 6000 horsepower, 3500 rpm AC induction motor (magenta) which is powered by a variable-frequency power supply system. A variable ratio gearbox (orange) is connected to the electric motor that supports rotational speeds up to 60,000 rpm, and the speed of the test article is maintained within 0.013% of the setpoint with feedback control from the variable frequency power system. The motor, gearbox, and collector are all mounted to a bedplate while the compressor is mounted to the vertical face of the collector.

The facility inlet system is shown in blue in Figure 1. The facility draws in atmospheric air from either a large filter housing located just outside the test cell, a 40-psig supply referred to as combustion air, or a 10-psig refrigerated air system. An orifice plate is used to measure the mass flow rate passing through the test article. The orifice plate is located downstream of all the inlet air supplies with 10 and 4 pipe diameters of straight pipe upstream and downstream of the measurement plane, respectively. Two inlet butterfly valves mounted in parallel, one each for coarse and fine adjustment, control the air pressure at the compressor inlet. The fine adjustment valve features a closed-loop feedback system to maintain a constant inlet air pressure. The air is then passed through a 60-inch diameter inlet plenum with two screens to provide uniform flow and reduce the flow velocity delivered to the bellmouth inlet just upstream of the compressor test section.

After work is done on the flow in the green compressor test section, air is discharged through the collector which houses an annular throttle valve with up to 8 discharge ports. The discharge ports can be plugged or left open as needed to accommodate the mass flow rate range of a given research article with a maximum mass flow rate of 65-lbm/sec and maximum temperature of 1300°F. The air is passed from the collector through the red exhaust pipe in Figure 1 where it is either cooled by a water spray and discharged to the atmosphere or, if the exhaust pressure is less than atmospheric pressure, to the NASA Glenn Altitude Exhaust System.

Separate lubrication packages serve the compressor, gearbox, and drive motor individually. All the systems are monitored for temperature, pressure, and flowrate and equipped with chip detectors as well as heaters. Each system is equipped with a pneumatic backup pump driven by an auxiliary air system that automatically engages upon detection of pressure loss by a pressure switch.

Auxiliary 125-psig air is supplied at numerous locations throughout the facility. In terms of aerodynamic performance, the auxiliary air supply is used in conjunction with a labyrinth seal to maintain the desired flowrate through the leakage path at the backface of the impeller.

A tip clearance control system allows for adjustment of the axial impeller position relative to the compressor shroud. The system supports tip clearance gaps from 0.009 inches to more than 0.050 inches at the impeller exducer at all operating conditions of interest and is able to maintain the desired condition with a precision of 0.0001 inches.

3. FACILITY DATA ACQUISITION SYSTEMS

Extensive instrumentation throughout the facility acquires facility health, static aerodynamic performance, and dynamic signal data. The legacy ESCORT system originally developed in the 1970s for data acquisition at NASA Glenn Research Center was used throughout the test campaigns documented in the present work. However, an upgrade of the data acquisition system is in process at the time of writing. As such, the present work will be focused on documentation of the forthcoming COBRA system. In conjunction with COBRA, which is used primarily for data acquisition, Wonderware is used for human-machine interface (HMI) to operate the facility. The overall instrumentation and data acquisition architecture is presented in Figure 2.

The majority of the facility health metrics in CE-18 are processed through programmable logic controllers (PLCs) to manage alarms, automatic shutdowns, and controls loops. The motor, gearbox, and compressor vibrations are monitored with accelerometers. The analog signals of the accelerometers are passed through a Bently Nevada 3500 chassis before reaching the PLC. The same communication string is also used for keyphasors and gearbox shaft orbits.

Digital Temperature Systems with K150 Ice Point References measure the majority of the temperatures in the facility, though some temperatures associated with operational limits are directly quantified by the PLC. Flow meters in the lubrication systems are also measured by the PLC. Pressure measurements are acquired with either Druck UNIK 5000 pressure transducers or a series of NetScanner 9816 modules paired with NetScanner 98RK-1 chassis. Pressure and temperature measurements collected by COBRA and the PLC are passed between the two systems via TCP/IP protocol as needed to support facility operation and data recording in the appropriate software platform. Finally, the necessary measurements passed through the PLC are displayed on Wonderware terminals for human machine interface. The Wonderware interface includes monitoring of critical measurements and aerodynamic performance. Operating conditions are maintained or changed by adjusting valves, such as the collector throttle or inlet valves, in the HMI. In some instances, such as setting of the differential pressure across the labyrinth seal at the impeller backface, control loops are used to maintain a constant setpoint.

The COBRA DAQ system measures the remaining steady instrumentation consisting of various pressure transducers and humidity measurements and processes the acquired data to display aerodynamic performance parameters both numerically and graphically. These displays may consist of tables of pressure readings for inspection during testing or real-time plots of the compressor map, spanwise profiles, component pressure rise, etc. These dataviewers are used in conjunction with the Wonderware HMI to set and maintain desired aerodynamic operating conditions.

Dynamic data streams are acquired on a separate computer connected to a DEWESoft system. The analog signals, usually generated by Kulite pressure transducers or strain gauges, are

first conditioned by the appropriate Precision Filter card housed in a 28000F chassis. The analog filters are set to slightly less than the Nyquist frequency of the DEWESoft system at the time of data acquisition. Generally, the sample frequency has been set to 200 kHz for digitization of dynamic pressure signals at stable operating conditions. When approaching instability, the sample frequency is reduced to ensure the data files do not become so large that their utility is degraded. The dynamic data is displayed with real-time waveforms and frequency content with a dedicated dynamic DAQ computer. Tip clearance measurements are processed and recorded separately from the rest of the dynamic data. A dedicated Capacisense system conditions, processes, and records clearance measurements which are passed to COBRA via an output voltage.

4. HECC CONFIGURATIONS AND INSTRUMENTATION

At the time of writing, there are two diffuser configurations and two inlet configurations available for the HECC test article. The design and testing of the original vaned diffuser

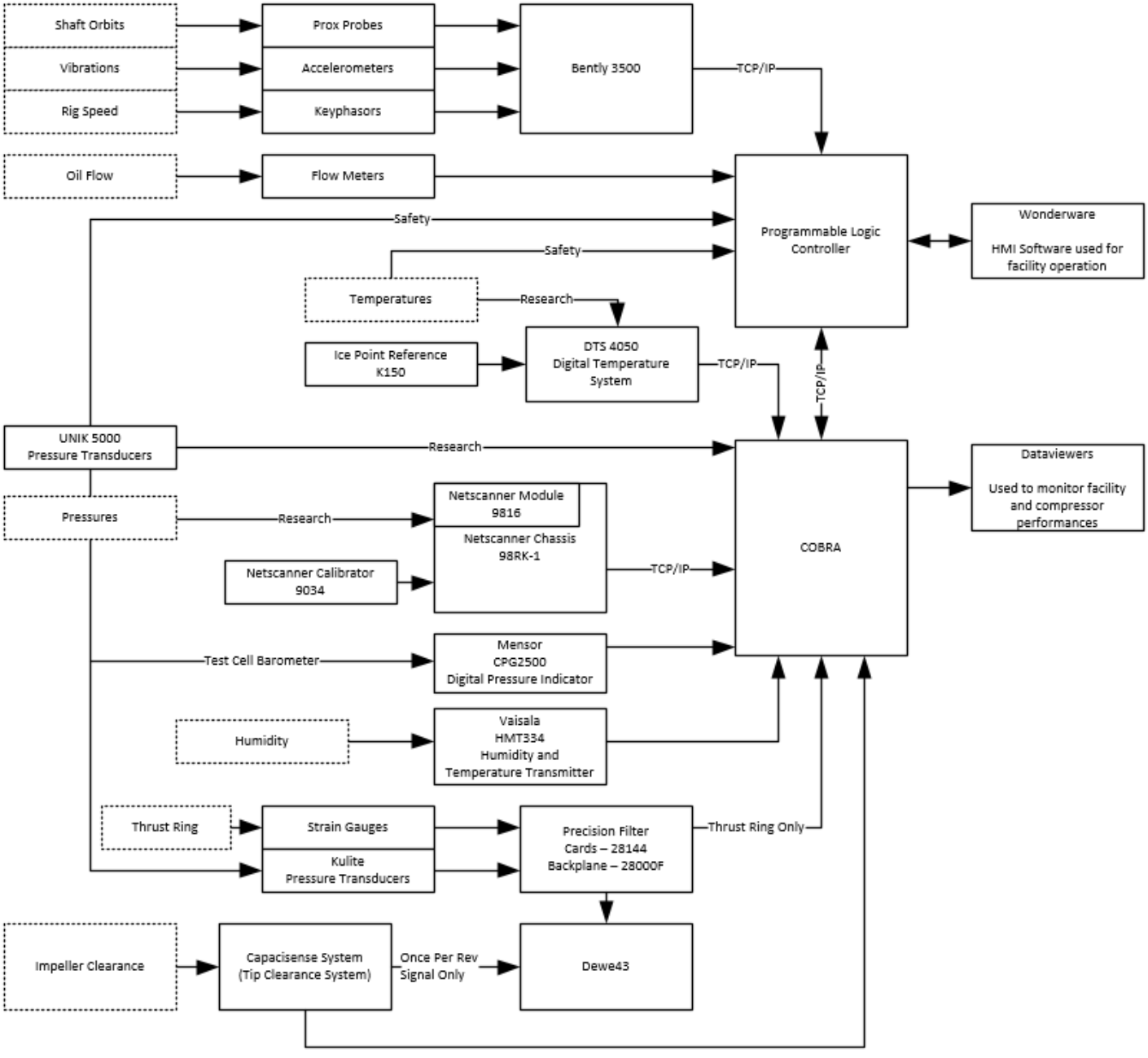

FIGURE 2. CE-18 DATA ACQUISITION AND MONITORING SYSTEM ARCHITECTURE.

configuration is documented in detail by Medic et al. [1]. In summary, the HECC goals were to increase both efficiency and loading coefficient relative to the predecessor compressor, CC3, while also reducing the maximum diameter of the stage and increasing surge margin. The final design intent performance included a stage pressure ratio of 4.85, inlet corrected mass flow rate of 11.2-lbm/s, loading coefficient of 0.79, and polytropic stage efficiency of 88.8%. Because the vaned diffuser configuration did not meet the aggressive performance benchmarks targeted in the design effort, the vaneless diffuser configuration was developed to provide the impeller with design-intent exit conditions and examine the impeller performance in isolation from the vaned diffuser.

Key geometric parameters of the HECC vaneless configuration are given in Table 1. Comparisons of the vaned diffuser, vaneless diffuser, and possible transition duct flow paths are given in Figure 3 and Figure 4 alongside the stage nomenclature. The station numbers are shared between the vaned and vaneless stages both for clarity and because many measurements in the vaneless diffuser configuration are collected at geometric locations that correspond to key locations in the vaned diffuser. For example, Station 3, which is the vaned diffuser leading edge (Figure 3), corresponds to the impeller exit rating plane in the vaneless diffuser configuration (Figure 4), and many key measurements are recorded at that radius in both configurations.

TABLE 1. GEOMETRIC PARAMETERS OF THE HECC IMPELLER.

Parameter	Value	Units
Blade Number	15/15	MB/SB
LE Tip Radius	4.73	in
LE Hub Radius	1.60	in
TE Radius	8.5	in
Backsweep	30	°
Exit Blade Height	0.61	in

To illustrate the geometric differences between the vaned and vaneless diffusers, both diffusers are drawn to scale with the vaneless diffuser overlaying the vaned diffuser in translucent gray in Figure 3. The vaneless diffuser includes a 30% shroud side pinch that extends to near the impeller trailing edge, and the area is constant from the end of the pitch to the bend. The area decreases by 5% over the axial distance of the annular duct downstream of the bend.

The two currently available configurations of the modular transition duct inlet, the baseline inlet and modified hub inlet, are shown in the same manner in Figure 4. The transition duct configuration features additively manufactured components such that various inlet flow paths can be swapped to examine the effects of the inlet flow path on the compressor performance and aerodynamics. At the time of writing, the baseline inlet and modified hub inlet have both been designed and tested. Additional configurations featuring inlet guide vanes and rotating inlet rakes were planned prior to the Covid-19 pandemic, but the scheduled testing was not completed due to delays and budgetary constraints associated with that event. The baseline inlet and modified hub inlet share the same shroud profile and converge to the same hub and shroud radii at the impeller leading edge, but the modified hub features a 0.5-inch increase in the hub radius at the nosecone, and thus, a more aggressive hub radius change from the nosecone hub to the impeller leading edge hub (Figure 4).

A meridional view of the instrumentation in the HECC vaneless diffuser configuration with the baseline inlet is given in Figure 5. The instrumentation in the vaned diffuser and modular

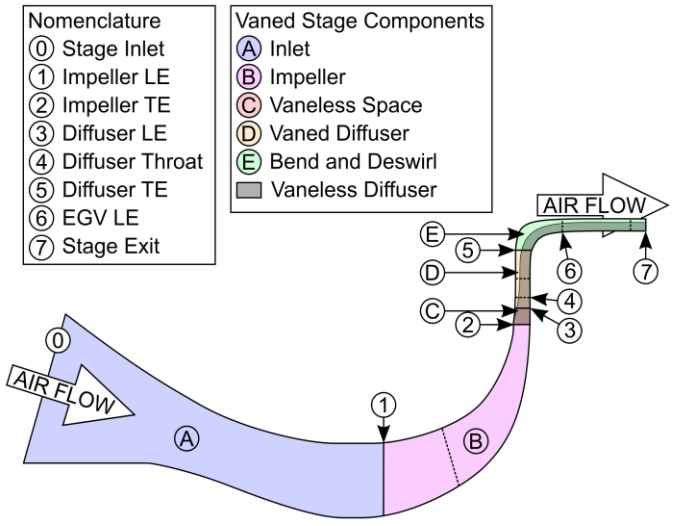

FIGURE 3. VANED AND VANELESS DIFFUSER CONFIGURATIONS OF HECC WITH NOMENCLATURE.

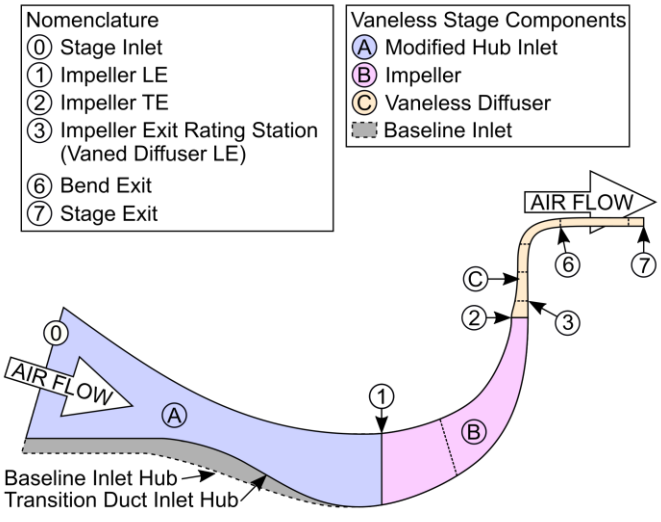

FIGURE 4. COMPARISON OF BASELINE INLET WITH MODIFIED HUB INLET IN HECC VANELESS DIFFUSER CONFIGURATION.

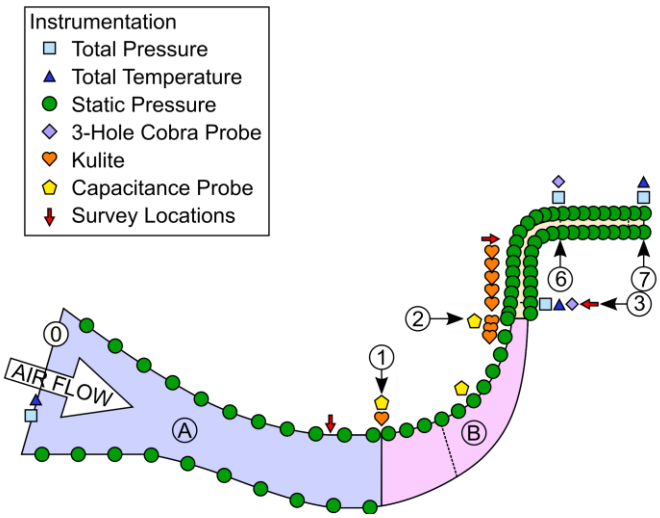

FIGURE 5. HECC VANELESS DIFFUSER INSTRUMENTATION.

hub configurations can also be approximated from the illustration in Figure 5. Modular vane inserts allow for various types of instrumentation to be placed just downstream of the impeller at Station 3. Total pressure and total temperature measurements are located at key points in the flow path to characterize the stage performance. The stage inlet total conditions and relative humidity are collected in the plenum upstream of the compressor at Station 0. Total pressure and temperature rakes are located just downstream of the impeller and at the stage exit, at Stations 3 and 7, respectively. Static pressures taps are distributed along the hub and shroud, and there are usually at least two measurements in different circumferential locations for each meridional location. Cobra probes of the three-hole type for calculation of flow angle can also be installed just downstream of the impeller and at the bend exit (Stations 3 and 6, respectively). At Station 6, the 3-hole probes are stationary in the flow path, while at Station 3 the 3-hole probes are installed in actuators with the modular vane inserts. The actuators are used to traverse the probe across the span to measure the flow angle at the impeller exit. Alternatively, the same traverse can be conducted with other standard probes having 0.25" diameter stems. In addition to the spanwise traverse downstream of the impeller, rotating rakes can be installed at the aerodynamic interface plane just upstream of the impeller leading edge in the transition duct configuration of the stage.

The dynamic instrumentation consists primarily of high-frequency pressure transducers and capacitance probes. Kulite high frequency pressure transducers are installed in the shroud at the impeller leading edge as well as from just upstream of impeller trailing edge through the radial portion of the vaneless diffuser. Three capacitance probes are installed along the impeller shroud for real-time quantification of the tip clearance at the inducer, knee, and exducer of the impeller. Since there is only one measurement of tip clearance at each meridional location, prior to each test campaign, rub probes are installed at four circumferential locations at the three meridional locations and the clearance is recorded at various operating conditions to understand the variation of the tip clearance around the circumference of the impeller.

Finally, metal temperatures along the compressor shroud and at the backface of the impeller are recorded but not explicitly shown in the illustration in Figure 5. The same is true of numerous static pressure taps also located at the impeller backface.

5. HECC VANELESS DIFFUSER CONFIGURATION BASELINE INLET PERFORMANCE

Steady compressor performance data were obtained between 75% and 100% corrected speed. The total pressure ratio (TPR), total temperature rise ratio (TTR), efficiency, and corrected mass flow rate are used to quantify the stage performance. Corrected speed and corrected mass flow rate are calculated using humid air and real gas properties retrieved from REFPROP [32], and the efficiency and uncertainty thereof are determined according to the procedures given by Lou et al. [33]. The present section discusses the performance of the HECC impeller and vaneless diffuser with the original, metal baseline inlet and the additively manufactured plastic replication of the baseline inlet, referred to as BLM (baseline metal) and BLP (baseline plastic), respectively, for brevity. Due to failure of total temperature rakes at the impeller exit during the initial BLM vaneless diffuser test, discussion in the present section is focused on the stage performance. The impeller performance will be considered in greater detail in Section 6.

The impeller exit total pressure profiles at Station 3, the vaned diffuser leading edge radius, at the design point are shown in Figure 6. The design operating condition of the HECC is 21,789-rpm and 11-lbm/s at standard day conditions. The redundant circumferential measurements are in good agreement

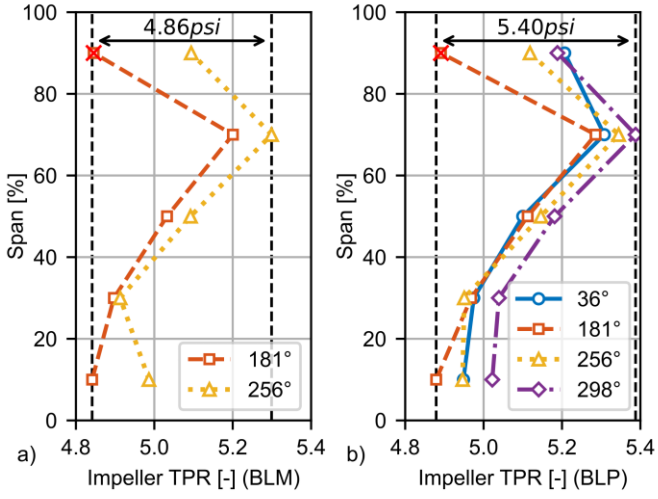

FIGURE 6. IMPELLER EXIT TOTAL PRESSURE PROFILES FOR (A) THE BASELINE METAL INLET AND (B) THE BASELINE PLASTIC INLET.

with each other in both the BLM and BLP configurations of the stage, and the maximum variation of total pressure in both configurations is less than 6-psi, most of which is due to spanwise rather than circumferential variation. In the proceeding performance evaluation, the total pressure element marked with a red X (at 181°, 90% span in Figure 6) is excluded from the calculations due to the significant difference it manifests compared to the measurements at the same span in the BLP configuration. Additional total pressure rakes were included in the BLP configuration to provide greater confidence in the experimental measurements. Throughout the paper, the hub and shroud of the passage are located at 0% and 100% span, respectively.

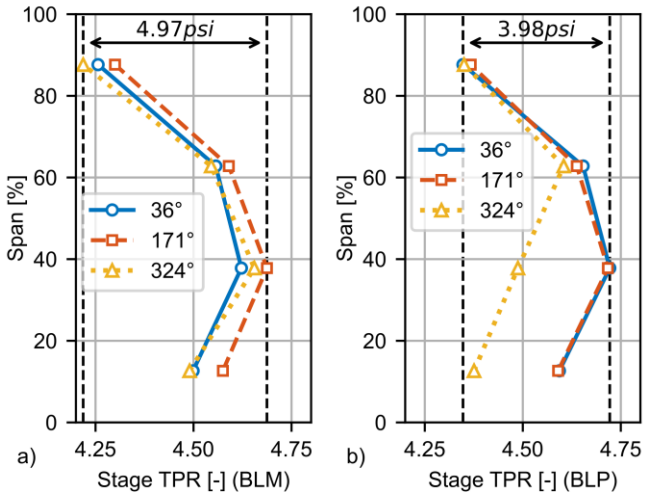

FIGURE 7. STAGE EXIT TOTAL PRESSURE PROFILES FOR (A) THE BASELINE METAL INLET AND (B) THE BASELINE PLASTIC INLET.

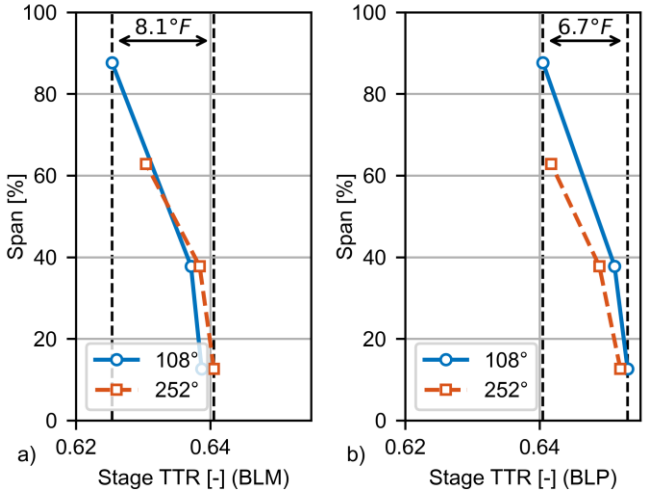

FIGURE 8. STAGE EXIT TOTAL TEMPERATURE PROFILES FOR (A) THE BASELINE METAL INLET AND (B) THE BASELINE PLASTIC INLET.

Total pressure and total temperature profiles at the HECC stage exit (Station 7) are given in Figure 7 and Figure 8, respectively. The spanwise profiles are in fairly good agreement around the circumference and between the BLM and BLP configurations. The discrepancy in the total pressure profile at the 324° rake for the BLP configuration arises in the BLM configuration, as well, though at slightly lower mass flow rates at 100% corrected speed. It is possible the discrepancy is due wakes shedding from the upstream impeller exit rakes. Regardless, the none of the stage exit total pressure elements were neglected.

Due to failure of a total temperature rake element, the near-span measurement at the 252° location is not included in the BLP configuration (Figure 8). Additionally, the total temperature measurement near 60% span, 108° location was also not included in performance calculations due to erratic readings during the test campaign. Profiles of the stage inlet conditions are not shown since they are based on four measurements (two total pressure and two total temperature) in the large volume inlet plenum upstream of the stage.

The HECC vaneless diffuser stage performance map is shown in Figure 9 for both the BLM and BLP inlet configurations. At all rotational speeds, the characteristics for each configuration overlay almost exactly and are within the uncertainty of the measurements. The uncertainty in total pressure ratio and mass flow rate are less than 0.55% and 0.78%, respectively, at all points. The mass flow rate was limited by the throttle rather than inducer choke during testing of the BLM inlet, so the throttle area was increased prior to the BLP testing by removing additional plugs from the throttle valve. While larger mass flow rates were achieved in the BLP configuration, inducer choke was approached only at 100% corrected speed as evidenced by the rapid drop in total pressure ratio above 12-

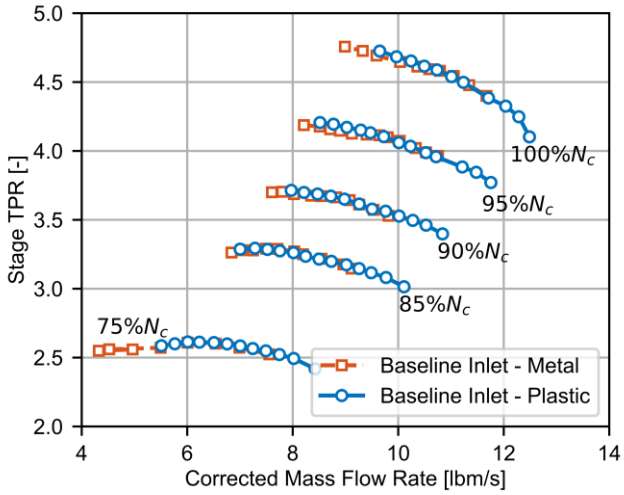

FIGURE 9. HECC IMPELLER PERFORMANCE MAP (VANELESS DIFFUSER CONFIGURATION).

lbm/s. As is typical of centrifugal compressors with vaneless diffusers, the HECC has a wide stable operating range at all of the tested rotational speeds. With increased risk of structural failure due to the plastic components in the BLP configuration, instability testing was only conducted with the BLM inlet. The differences in the minimum mass flow rates shown for each inlet are consequences of safety considerations and are not effects of the different inlet configurations.

The stage work plot (quantified with the total temperature rise ratio) of the HECC in the vaneless diffuser configuration is presented in Figure 10. The work input measured in the BLM configuration is slightly higher at all measured operating conditions. The difference in the measured TTR is partially due to the incorporation of real time humidity corrections between the BLM and BLP tests. Post-test humidity corrections for the BLM configurations resulted in a consistent undershoot of the intended corrected speed by 0.3-0.4%. As such, slightly lower corrected speeds resulting in less work input account for a portion of the reduction in TTR between the BLM and BLP testing. Additionally, although the maximum uncertainty in TTR is less than 1%, the remaining difference in TTR between the configurations should be within the combined uncertainty of the operating points.

The efficiency of the stage at 85%, 90%, 95%, and 100% corrected speeds is given in the subplots in Figure 11. The stage has a wide high efficiency operating range at 85% and 90% corrected speed, but at 95% and 100% corrected speed the peaks in efficiency are narrower and emerge at 10-lbm/s and 11-lbm/s, respectively. The difference in efficiency between the inlet configurations at all speeds is fairly small. There is some divergence on the high mass flow rate side of the 100% corrected speed characteristic, but a portion of the deviation may be attributed to the previously discussed undershoot of the humidity corrected speed during the BLM test campaign. At 100% corrected speed, the relative uncertainty in efficiency is between

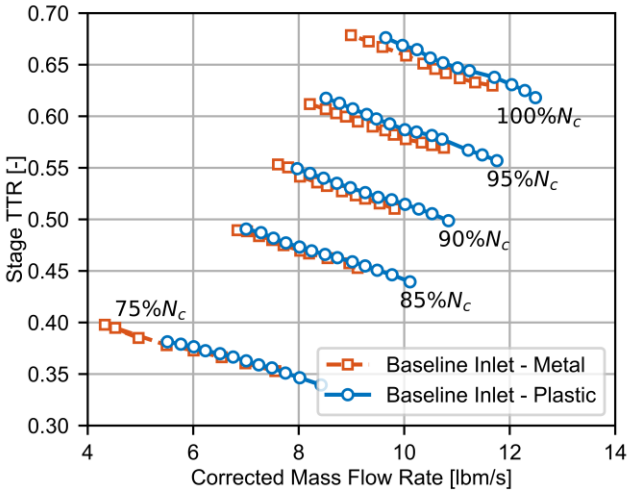

FIGURE 10. HECC VANELESS DIFFUSER CONFIGURATION STAGE WORK INPUT.

5.3% and 6.2%, though at off-design the uncertainty values approach nearly 10%. The large values of uncertainty for efficiency are typical when using real gas properties using the approach given by Lou et al. [33], such as the values reported in [34]. Despite the relatively large values of relative uncertainty, the repeatability of the pressure and temperature measurements from which the efficiency is calculated gives confidence that the reported values are representative of the flow field.

6. EFFECT OF S-DUCT ON IMPELLER PERFORMANCE

The area schedule of the modified hub (MH) inlet configuration is compared to that of the baseline inlet in Figure 12a. The left ordinate and abscissa are equal in aspect ratio to give a scale representation of the inlet. The axial coordinate, x, and the radial coordinate at a given axial location, r_x, are normalized by the mean radius at the impeller leading edge, $r_{1,mean}$. The impeller leading edge is located at a normalized duct length value of 0. The area ratio of the duct, given in terms of the area at a given axial location (A_x) normalized by the area at the impeller leading edge (A_1), is also included on the right-side ordinate. The larger hub radius of the MH inlet results in a greater change in radius between -2 and -1 of the normalized duct length coordinate. Because the shroud endwall contour is common between the inlet configurations, the difference in the duct area ratio is constant upstream of normalized duct length values approximately less than -2. The area ratio of the MH inlet hub then rapidly converges to the area ratio of the BLP inlet since the impeller leading edge geometry is unchanged by the inlet configuration.

An aerodynamic comparison of the BLP and MH inlet configurations is made using static pressure measurements at the shroud normalized by the inlet total pressure at the HECC design

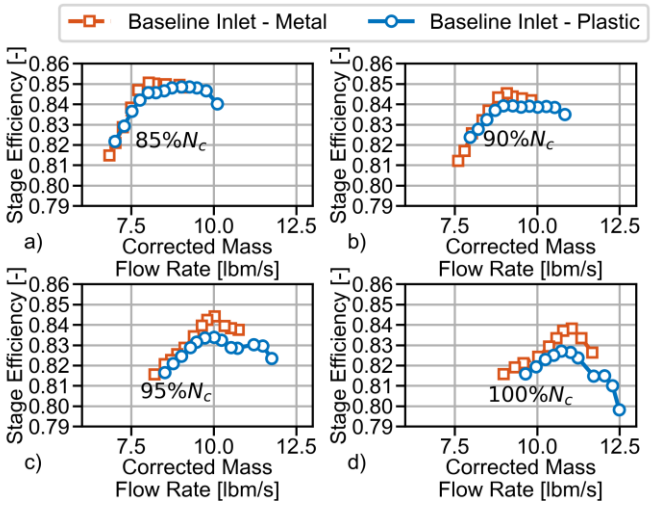

FIGURE 11. HECC VANELESS DIFFUSER CONFIGURATION ISENTROPIC STAGE EFFICIENCY AT A) 85%, B) 90%, C) 95%, AND D) 100% CORRECTED SPEED.

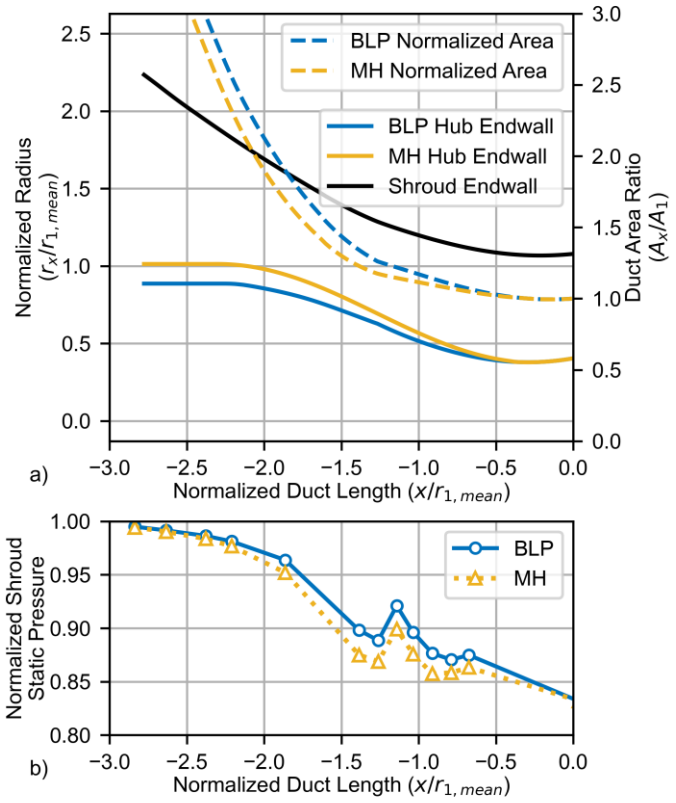

FIGURE 12. A) GEOMETRY AND AREA PROFILES OF THE BASELINE AND MODIFIED HUB INLET CONFIGURATIONS AND B) NORMALIZED SHROUD STATIC PRESSURE DEVELOPMENT.

point (100% corrected speed, 11-lbm/s) in Figure 12b. The normalized static pressure of the MH inlet decreases more rapidly through the duct because the area is smaller than that of the BLP inlet at the same axial location. The difference in the normalized static pressure between the inlet configurations is nearly constant once the area ratios converge at a normalized duct length value of approximately -1, and at the impeller leading edge the difference in normalized static pressure is approximately 1.5%.

Throughout the compressor map, the HECC impeller total pressure ratio is almost unchanged by more rapid acceleration of the flow in the MH inlet configuration, Figure 13. Some slight deviation in total pressure ratio is present at 100% corrected speed, but the differences are within the uncertainty of the measurements. Comparing the total pressure ratio of the impeller alone to that of the stage in Figure 9, the impeller total pressure is approximately 10% greater than that of the impeller and vaneless diffuser together at the same corrected speeds and mass flow rates.

The difference in the impeller efficiency between the inlet configurations is small enough that it is likely statistically insignificant, Figure 14. While the difference in efficiency between the inlet configurations is negligible, the impeller

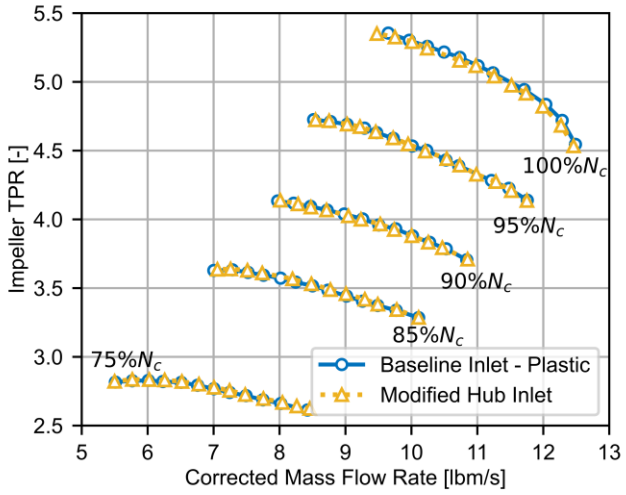

FIGURE 13. HECC IMPELLER TOTAL PRESSURE RATIO IN THE BLP AND MH INLET CONFIGURATIONS.

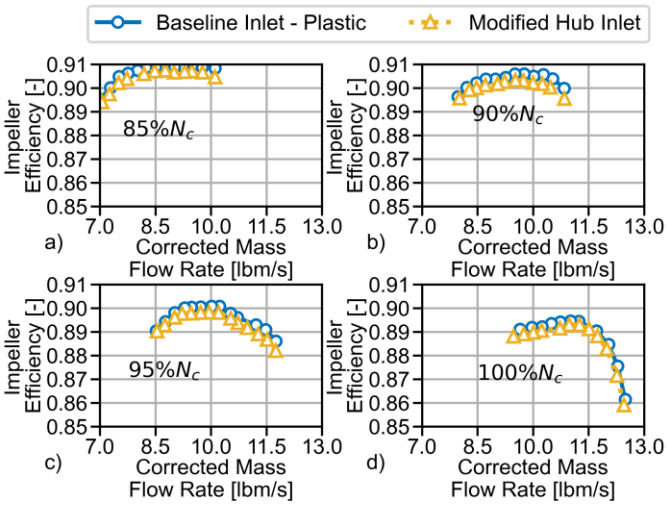

FIGURE 14. HECC IMPELLER ISENTROPIC EFFICIENCY IN THE BLP AND MH INLET CONFIGURATIONS.

efficiency measurements show wider efficient operating ranges for the impeller alone compared to the entire stage (Figure 11) at all speeds. The efficiency falls off rapidly at 100% speed due to inducer choke (Figure 14d), but there is less than a 0.5% drop from the peak efficiency point near 11-lbm/s to the minimum recorded mass flow rate recorded with the additively manufactured inlets.

Based on the performance measurements in Figure 13 and Figure 14, the HECC impeller is robust to the changes in the inlet flow field brought about by the MH inlet. This is likely due to the small effect of the MH inlet on the inlet flow field itself (Figure 12) combined with the general robustness of centrifugal

compressors to the presence of inlet distortion. While the observations presented herein are not conclusive for all designs or applications, S-duct type inlets typical of axi-centrifugal compressors or turboelectric engine architectures do not appear to be a primary concern for centrifugal compressor performance going forward.

7. PUBLIC ACCESS

All currently available diffuser and inlet configurations of the HECC are open, and the geometry, performance, and detailed aerodynamic data have been made available for download at the NASA High Efficiency Centrifugal Compressor Data Archive which is accessible via this public link: https://storage.googleapis.com/hecc-data/NASA-HECC-Data-Archive.zip [35]. A detailed read-me file is included to simplify usage of the data, and interested parties are encouraged to reach out to the authors as needed.

At the time of writing, the archive contains a compressed, downloadable file with the vaned diffuser configuration experimental data, blade sections, and a solid model of the stage. The hub and shroud endwalls published in the HECC design report [1] are also available there. It should be noted, however, that the blade sections from the design report do not include the fillets on the impeller, diffuser, or exit guide vanes.

The experimental data for the vaneless diffuser stage and both inlet configurations, which are discussed throughout this report, as well as the solid models, are also included in the archive. The experimental data consists of overall performance metrics as well as detailed measurements, such as static pressures, throughout the compressor stage. The hub and shroud endwall coordinates of the vaneless diffuser are also hosted in the archive.

Work is ongoing to provide updated blade sections including fillets on all components. This archive will be maintained and updated with additional datasets as they are acquired and published.

8. CONCLUSIONS

Extensive, varied, high-quality experimental data are necessary to continue the advancement of gas turbines to new and complex engine architectures for future aircraft. While computational approaches for compressor modeling have achieved greater insight and accuracy over recent years, experimental data remains necessary for tool validation and development. The HECC test article in the Small Engine Components Compressor Test Facility at NASA Glenn Research Center is equipped to provide open, non-normalized datasets to support these efforts.

The steady performance of the HECC vaneless diffuser configuration with three different inlet configurations has been presented with emphasis on discussion of the overall performance of the vaneless diffuser stage as well as the impeller alone. Minimal differences were observed between the original metal inlet (BLM configuration) and the plastic, additively manufactured replication of the original metal inlet (BLP configuration). Furthermore, the HECC impeller performance was robust to the more aggressive radius change in the additively manufactured modified hub inlet (MH configuration). Spanwise profiles throughout the stage showed good uniformity between measurements and repeatability of stage metrics gives confidence in quantification of the impeller and stage performance.

Data for interrogation of the effects of tip clearance on the impeller performance and investigation of the development of instability in the vaneless diffuser configuration have been acquired and are being analyzed at the time of writing. Planned future work includes optical access modification to acquire velocity data in the vaned diffuser downstream of the impeller.

ACKNOWLEDGMENTS

This effort is sponsored by the Revolutionary Vertical Lift Technology Project of the NASA Advanced Air Vehicles Program. The authors would like thank Raytheon Technologies Research Center for the design work on the HECC vaneless diffuser configuration. The support of Mr. Jozsef Puskas, Mr. Alex Camargo, Mr. Jacob Jaksic, and Mr. Jonathan Mitchell in conducting experiments in the Small Engine Components Compressor Test Facility is gratefully acknowledged. The authors are also grateful to Mr. David Na for his help setting up the publicly accessible data archive.

REFERENCES

[1] Medic, G., Sharma, O. P., Jongwook, J., Hardin, L. W., McCormick, D. C., Cousins, W. T., Lurie, E. A., Shabbir, A., Holley, B. M., and Van Slooten, P. R., 2017, *High Efficiency Centrifugal Compressor for Rotorcraft Applications*, E-18856-1.

[2] Gooding, W. J., Meier, M. A., and Key, N. L., 2021, "The Impact of Various Modeling Decisions on Flow Field Predictions in a Centrifugal Compressor," J. Turbomach., **143**(10).

[3] Ziegler, K. U., Gallus, H. E., and Niehuis, R., 2003, "A Study on Impeller-Diffuser Interaction—Part I: Influence on the Performance," J. Turbomach., **125**(1), p. 173.

[4] Dean, R. C., and Senoo, Y., 1960, "Rotating Wakes in Vaneless Diffusers," J. Basic Eng., **82**(3), pp. 563–570.

[5] Eckardt, D., 1978, *Investigation of the Jet-Wake Flow of a Highly Loaded Centrifugal Compressor Impeller*, NASA TM-75232, NASA, Washington, D.C.

[6] Krain, H., 1988, "Swirling Impeller Flow," J. Turbomach., **110**(1), pp. 122–128.

[7] Skoch, G. J., Prahst, P. S., Wernet, M. P., Wood, J. R., and Strazisar, A. J., 1997, "Laser Anemometer Measurements of the Flow Field in a 4:1 Pressure Ratio Centrifugal Impeller," American Society of Mechanical Engineers, p. V001T03A049.

[8] Ibaraki, S., Matsuo, T., and Yokoyama, T., 2007, "Investigation of Unsteady Flow Field in a Vaned Diffuser of a Transonic Centrifugal Compressor," J. Turbomach., **129**(4), pp. 686–693.

[9] Dawes, W. N., 1995, "A Simulation of the Unsteady Interaction of a Centrifugal Impeller With Its Vaned

Diffuser: Flow Analysis," J. Turbomach., **117**(2), pp. 213–222.
[10] Bryan, W. B., 1991, "An Investigation of Unsteady Impeller-Diffuser Interactions in a Centrifugal Compressor," Ph.D., Purdue University.
[11] Krain, H., 2002, "Unsteady Diffuser Flow in a Transonic Centrifugal Compressor," Int. J. Rotating Mach., **8**(3), pp. 223–231.
[12] Ziegler, K. U., Gallus, H. E., and Niehuis, R., 2003, "A Study on Impeller-Diffuser Interaction—Part II: Detailed Flow Analysis," J. Turbomach., **125**(1), p. 183.
[13] Shum, Y. K. P., Tan, C. S., and Cumpsty, N. A., 2000, "Impeller–Diffuser Interaction in a Centrifugal Compressor," J. Turbomach., **122**(4), pp. 777–786.
[14] Toyama, K., Runstadler, P. W., and Dean, R. C., 1977, "An Experimental Study of Surge in Centrifugal Compressors," J. Fluids Eng., **99**(1), pp. 115–124.
[15] Hunziker, R., and Gyarmathy, G., 1994, "The Operational Stability of a Centrifugal Compressor and Its Dependence on the Characteristics of the Subcomponents," J. Turbomach., **116**(2), pp. 250–259.
[16] Skoch, G. J., 2003, "Experimental Investigation of Centrifugal Compressor Stabilization Techniques," J. Turbomach., **125**(4), pp. 704–713.
[17] Spakovszky, Z. S., 2004, "Backward Traveling Rotating Stall Waves in Centrifugal Compressors," J. Turbomach., **126**(1), p. 1.
[18] Everitt, J. N., and Spakovszky, Z. S., 2013, "An Investigation of Stall Inception in Centrifugal Compressor Vaned Diffuser," J. Turbomach., **135**(1), p. 011025.
[19] He, X., and Zheng, X., 2018, "Flow Instability Evolution in High Pressure Ratio Centrifugal Compressor with Vaned Diffuser," Exp. Therm. Fluid Sci., **98**, pp. 719–730.
[20] Sun, Z., Zheng, X., and Kawakubo, T., 2018, "Experimental Investigation of Instability Inducement and Mechanism of Centrifugal Compressors with Vaned Diffuser," Appl. Therm. Eng., **133**, pp. 464–471.
[21] Lou, F., Harrison, H. M., and Key, N. L., 2022, "Investigation of Surge in a Transonic Centrifugal Compressor With Vaned Diffuser: Part I—Surge Signature," J. Turbomach., **145**(5).
[22] Lou, F., Harrison, H. M., Brown, W. J., and Key, N. L., 2022, "Investigation of Surge in a Transonic Centrifugal Compressor With Vaned Diffuser: Part II—Correlation With Subcomponent Characteristics," J. Turbomach., **145**(5).
[23] Galloway, L., Spence, S., In Kim, S., Rusch, D., Vogel, K., and Hunziker, R., 2018, "An Investigation of the Stability Enhancement of a Centrifugal Compressor Stage Using a Porous Throat Diffuser," J. Turbomach., **140**(1), p. 011008.
[24] Lou, F., Fabian, J. C., and Key, N. L., 2019, "Design Considerations for Tip Clearance Sensitivity of Centrifugal Compressors in Aeroengines," J. Propuls. Power, **35**(3), pp. 666–668.
[25] Pfleiderer, C., 2013, *Die Kreiselpumpen für Flüssigkeiten und Gase: Wasserpumpen, Ventilatoren, Turbogebläse Turbokompressoren*, Springer-Verlag.
[26] Eckert, B., and Schnell, E., 2013, *Axial-Und Radialkompressoren: Anwendung/Theorie/Berechnung*, Springer-Verlag.
[27] Hall, D. K., Greitzer, E. M., Uranga, A., Drela, M., and Pandya, S. A., 2022, "Inlet Flow Distortion in an Advanced Civil Transport Boundary Layer Ingesting Engine Installation," J. Turbomach., **144**(10).
[28] Gunn, E. J., and Hall, C. A., 2014, "Aerodynamics of Boundary Layer Ingesting Fans," *ASME Turbo Expo 2014: Turbine Technical Conference and Exposition*, American Society of Mechanical Engineers, p. V01AT01A024-V01AT01A024.
[29] Sheoran, Y., Bouldin, B., and Krishnan, P. M., 2012, "Compressor Performance and Operability in Swirl Distortion," J. Turbomach., **134**(4), p. 041008.
[30] Lavan Kumar, G., Vunnam, K., Bouldin, B., and Sheoran, Y., 2013, "Investigation of Plenum Inlet Distortion and Its Impact on Compressor Total Pressure and Swirl Distortion," American Society of Mechanical Engineers Digital Collection.
[31] Brokopp, R., and Gronski, R., 1992, "Small Engine Components Test Facility Compressor Testing Cell at NASA Lewis Research Center," American Institute of Aeronautics and Astronautics, Nashville, TN.
[32] Lemmon, E. W., Bell, I. H., Huber, M. L., and McLinden, M. O., 2018, "NIST Standard Reference Database 23: Reference Fluid Thermodynamic and Transport Properties-REFPROP, Version 10.0, National Institute of Standards and Technology."
[33] Lou, F., Fabian, J., and Key, N. L., 2014, "The Effect of Gas Models on Compressor Efficiency Including Uncertainty," J. Eng. Gas Turbines Power, **136**(1), p. 012601.
[34] Lou, F., Harrison, H. M., Fabian, J. C., Key, N. L., James, D. K., and Srivastava, R., 2016, "Development of a Centrifugal Compressor Facility for Performance and Aeromechanics Research," *Seoul, South Korea*, American Society of Mechanical Engineers Digital Collection.
[35] Harrison, H. M., 2022, "NASA HECC Data Archive," NASA [Online]. Available: https://storage.googleapis.com/hecc-data/NASA-HECC-Data-Archive.zip.